Spectral engineering of entangled two-photon states

Silvia Carrasco, Alexander V. Sergienko, Bahaa E. A. Saleh, and Malvin C. Teich
Quantum Imaging Laboratory, Department of Electrical and Computer Engineering and Department of Physics, Boston University, 8 Saint Mary's Street, Boston, Massachusetts 02215, USA

Juan P. Torres and Lluis Torner
ICFO-Institut de Ciencies Fotoniques and Universitat Politecnica de Catalunya, Mediterranean Technology Park, 08860 Castelldefels (Barcelona), Spain

(Received 5 October 2005; revised manuscript received 21 February 2006; published 2 June 2006)

We experimentally demonstrate an approach for manipulating the spectral profiles of entangled-photon pairs. The spectral properties are determined by selecting both the appropriate spatial profile of the pump laser radiation and the geometry of the noncollinear spontaneous parametric downconversion. Both spectra, the spectrum of the individual signal and idler photons, and the joint spectrum of the entangled-photon pairs, can be modified at will over a substantial range of values. This technique is therefore expected to be useful for an array of quantum-optics applications.

DOI: 10.1103/PhysRevA.73.063802 PACS number(s): 42.50.Ar, 42.50.Dv, 42.65.Ky

I. INTRODUCTION

One of the most widely used technologies in quantum communication science for generating entangled-photon pairs is spontaneous parametric down conversion (SPDC) [1]. Entangled photons generated by SPDC can exhibit nonclassical correlations in several observables, such as frequency, polarization, and momentum [2].

A key ingredient in the implementation of any quantum scheme is the feasibility of manipulating the corresponding properties of the quantum state. Polarization-entangled states have been manipulated in various experiments (see, for example, [3–5]). The spatial shape of momentum-entangled states has been tailored for applications in quantum imaging [6–9], for concentration of entanglement in higher-dimensional Hilbert spaces [10], and for modifying the two-photon interference behavior in a Hong-Ou-Mandel interferometer [11].

However, despite the needs for specific spectral shapes of frequency-entangled photon pairs in various quantum-optics applications, few experiments have been devoted to manipulating these spectra, except for the prolongation of the correlation time that arises from the use of narrowband filters [12–15], and the time shaping that follows from the use of Fourier-conjugated spectral-phase manipulations [16].

These requirements extend from the need for narrowband entangled states (for minimizing the chromatic dispersion in long-distance quantum cryptography schemes, for example, [17]) to the need for ultrabroadband states (for maximizing the resolution in quantum optical coherence tomography, for example, [18]). Other cases are the suppression of spectral information [19], and the control of the photon correlations (for improving the accuracy of clock synchronization [20] or performing linear-optical logic operations [21], as examples). The tailoring of spectra associated with spontaneous parametric down conversion is therefore an important goal.

In noncollinear SPDC, where the pump, signal, and idler photons do not propagate along the same direction, the spectrum of the generated entangled-photon pairs can be manipulated, without the need for spectral shapers, by simply modifying the spatial shape of the pump beam [22–26].

In this paper, we experimentally demonstrate the feasibility of this approach. We show that noncollinear geometries, in combination with pump spatial profile manipulation, offer new features and opportunities for controlling the spectral properties of the entangled two-photon pairs, as well as for tailoring the spectra of the individual photons.

II. THEORY

We consider a laser pump beam incident in a quadratic nonlinear optical crystal of length L, propagating in the z direction, where $\mathbf{x}=(x,y)$ is the position in the transverse plane. We also define a more convenient coordinate system: $x_{1,2}=x$, $y_{1,2}=y\cos\varphi_{1,2}+z\sin\varphi_{1,2}$ and $z_{1,2}=z\cos\varphi_{1,2}-y\sin\varphi_{1,2}$, where $\varphi_{1,2}$ are the angles formed by the direction of propagation of the pump beam, z, and the direction of propagation of the signal, z_1, and idler photons, z_2, respectively. Applying the formalism of Ref. [22], while restricting ourselves to the case of a continuous wave (cw) pump and neglecting the effects of Poynting vector walk-off, the quantum state of the two photons is given by

$$|\Psi\rangle = \int d\omega_s d\omega_i d\mathbf{p} d\mathbf{q} \Phi(\omega_s,\omega_i,\mathbf{p},\mathbf{q}) \hat{a}_s^\dagger(\omega_s,\mathbf{p}) \hat{a}_i^\dagger(\omega_i,\mathbf{q}) |0,0\rangle, \tag{1}$$

where the state function is [22,27]

$$\Phi(\omega_s,\omega_i,\mathbf{p},\mathbf{q}) = \bar{E}_p(p_x+q_x,\Delta_0)\mathrm{sinc}(\Delta_k L/2)\exp(-i\Delta_k L/2). \tag{2}$$

In this expression, $\mathbf{p}=(p_x,p_y)$ is the transverse momentum for the signal photon, $\mathbf{q}=(q_x,q_y)$ is the transverse momentum of the idler photon, $\bar{E}_p(\mathbf{q}_p)$ represents the amplitude distribution of the pump beam in momentum space (the spatial Fou-

rier transform), $\Delta_0 = p_y \cos\varphi_1 + q_y \cos\varphi_2 - k_s \sin\varphi_1 - k_i \sin\varphi_2$ follows from the phase-matching condition along the transverse y direction, $\Delta_k = k_p - k_s \cos\varphi_1 - k_i \cos\varphi_2 - p_y \sin\varphi_1 - q_y \sin\varphi_2$ comes from the phase-matching condition along the longitudinal z direction, and

$$k_p = [(\omega_p^0 n_p/c)^2 - (p_x + q_x)^2 - (\Delta_0)^2]^{1/2}. \quad (3)$$

Here, ω_p^0 is the angular frequency of the pump beam, n_p is the refractive index at the pump wavelength, and $k_{s,i}(\mathbf{p}) = [(\omega_s n_s/c)^2 - |\mathbf{p}|^2]^{1/2}$ are the longitudinal wave numbers of the signal and idler photons, respectively. The signal and idler frequencies are written as $\omega_s = \omega_s^0 + \Omega_s$ and $\omega_i = \omega_i^0 + \Omega_i$, respectively, where $\omega_{s,i}^0$ are the central frequencies, and $\Omega_{s,i}$ are the angular frequency deviations about the central frequencies. For a cw pump beam, the central frequencies satisfy $\omega_p^0 = \omega_s^0 + \omega_i^0$ together with $\Omega_i = -\Omega_s$.

In our experimental configuration, we collocate apertures far from the output face of the nonlinear crystal, in front of the detectors. If we assume that the Fraunhofer approximation [28] holds for the propagation of the signal and idler photons, the sought-after spectral spectral density $S_c(\Omega_s)$ of the two-photon state is given by

$$S_c(\Omega_s) \propto \int_A d\mathbf{x}_1 d\mathbf{x}_2 \left| \Phi\left(\Omega_s, -\Omega_s, \frac{\mathbf{x}_1}{\lambda_s^0 z_1}, \frac{\mathbf{x}_2}{\lambda_i^0 z_2}\right)\right|^2, \quad (4)$$

where A is the typical size (diameter) of the apertures, $\mathbf{x}_1$ and $\mathbf{x}_2$ are the transverse positions in the detection plane, $z_1 = z_2 = z_0$ are the propagation distances of the signal and idler photons from the output face of the nonlinear crystal, and λ_s^0 (λ_i^0) is the central wavelength of the signal (idler) photon.

The important role played by the spatial distribution of the two-photon state function in determining the spectral density appears in Eq. (4). If the probability of detecting a signal photon with angular frequency $\omega_s^0 + \Omega_s$ in coincidence with an idler photon with angular frequency $\omega_i^0 - \Omega_s$ at the detection plane is not correlated with the transverse positions $\mathbf{x}_1$ and $\mathbf{x}_2$, the spectral density of the two-photon state can be written as

$$S_c(\Omega_s) \propto |\Phi(\Omega_s, -\Omega_s, \mathbf{x}_1 = \mathbf{0}, \mathbf{x}_2 = \mathbf{0})|^2. \quad (5)$$

Generally speaking, this is the case for focused pump beams, namely $w_0 \ll (\lambda_s^0 z_0)/A$.

Expression (5) can be written as [22]

$$S_c(\Omega_s) \propto |\bar{E}_p(0, \alpha\Omega_s)|^2 \mathrm{sinc}^2\left\{\frac{(\beta\Omega_s + \gamma\Omega_s^2)L}{2}\right\}, \quad (6)$$

where α, β, and γ are parameters dependent on the crystal properties, defined as $\alpha = N_s \sin\varphi_1 - N_i \sin\varphi_2$, $\beta = N_i \cos\varphi_2 - N_s \cos\varphi_1$, and $\gamma = \frac{1}{2} M_s \cos\varphi_1 + \frac{1}{2} M_i \cos\varphi_2$ and $N_{s,i}$, and $M_{s,i}$ are the corresponding inverse group velocity and group velocity dispersion parameters at the signal (idler) frequencies, respectively.

Equation (6) demonstrates the potential for spectral engineering of the entangled-two-photon states offered by spatial pump manipulation in a noncollinear configuration. The spectral shape of the entangled two-photon state can be tailored by using the shape of the input pump beam, the length and dispersion properties of the nonlinear crystal, and the noncollinear angles chosen for propagation, in accordance with the central results of Ref. [22].

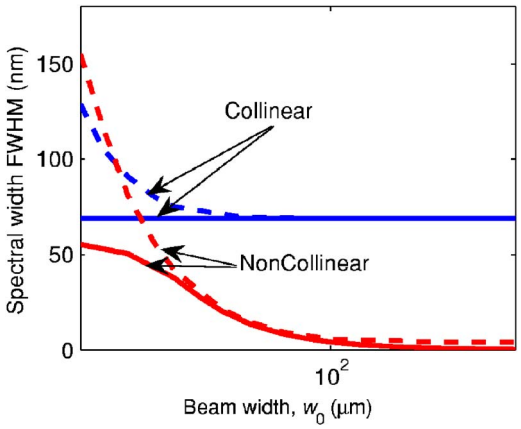

FIG. 1. (Color online) Calculated spectral width (FWHM) of the down converted photons vs the pump beam width w_0 for two different detection schemes. Solid curves: coincidence-detection scheme. Dashed curves: single-photon detection scheme. Two selected signal and idler output angles, $\varphi_1 = -\varphi_2 = 0°$ (collinear case), and $\varphi_1 = -\varphi_2 = 9°$ (noncollinear case) are compared for each regime. The twin photon source is a $LiIO_3$ sample of length $L = 1.5$ mm. The pump beam, of wavelength $\lambda_p^0 = 406$ nm, is taken to be Gaussian.

On the other hand, the spectrum of the individual signal and idler photons is given by

$$S_s(\Omega_s) \propto \int d\mathbf{x}_2 |\Phi(\Omega_s, -\Omega_s, \mathbf{x}_1 = \mathbf{0}, \mathbf{x}_2)|^2, \quad (7)$$

where we assume that the conditions validating the use of Eq. (5) hold as well.

The different results expected in the two detection schemes are summarized in Fig. 1, where we have plotted the spectral width as a function of the spatial width for an input Gaussian pump beam of beam waist ω_0. We consider both the joint spectrum of the two-photon pairs (solid curves), as given by Eq. (5) or Eq. (6), and the spectrum of the individual photons (dashed curves), as given by Eq. (7). A collinear and a noncollinear phase-matched SPDC configuration of angle $\varphi_1 = -\varphi_2 \simeq 9°$ is displayed in each case.

As was shown in [22] for the collinear case, the spectral width of the two-photon quantum state given by Eq. (5) is determined by the crystal properties, being independent of the pump beam waist. However, noncollinearly phase-matched SPDC configurations allow management of the spectral width from a few nm to a maximum spectral width corresponding to the collinear case. The collinear case constitutes the upper limit for the achievable spectral width.

However, this does not hold in the single-photon detection scheme described by Eq. (7). The spectral widths of the individual signal or idler photons depend on the properties of the input pump beam for the collinearly phase-matched SPDC configuration where a tightly focused pump beam allows the generation of very broad spectra [29]. The bandwidth corresponding to the collinear SPDC case is no longer the upper limit for the maximum achievable bandwidth.

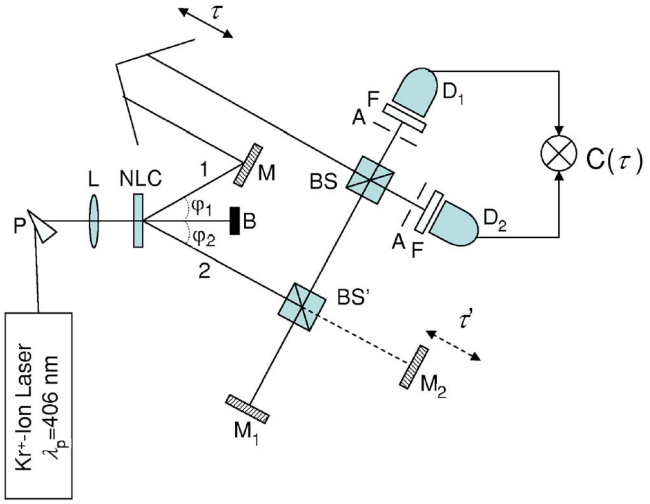

FIG. 2. (Color online) Experimental arrangement.

Noncollinear configurations can provide enhanced spectral widths. Moreover, as we will see subsequently, we have found that for particular angles, double-peaked signal or idler spectra can be obtained with a simple Gaussian beam at the input.

III. EXPERIMENT

The experimental setup is sketched in Fig. 2. Light from a monochromatic cw Kr^+-ion laser, operated at a wavelength $\lambda_p=406$ nm, and with a total power of 50 mW, after passing through a prism (P), and an aperture (not shown) to remove the spontaneous glow of the laser tube, pumps a 1.5-mm-long type-I $LiIO_3$ nonlinear crystal, cut at $\theta=41.7°$ for degenerate collinear phase matching. Proper rotation of the nonlinear crystal allows phase matching at the desired noncollinear angle.

Lenses of different focal lengths are placed before the crystal to control the input pump beam waist. All optical components of the system were selected to provide optimal performance in the 400–1000 nm wavelength range. For our particular system, the typical power at the detector was of the order of pW. However, output powers of the order of several μW can be obtained by using optimized SPDC sources, such as those that employ periodically poled materials with large effective nonlinearities and pumped with higher power lasers [16].

For the spectral characterization of the entangled two-photon state, the signal and idler beams, of central wavelength $\lambda_0=812$ nm, are directed into a Hong, Ou, and Mandel interferometer where two-photon interference is carried out. A temporal delay τ is inserted in the path of one of the beams (labeled as beam 1 in Fig. 2). Beam 2 is reflected from mirror M_1. Mirror M_2 is blocked in this case. The two photons, represented by beams 1 and 2, are then directed to the two input ports of a symmetric beam splitter (BS). The outputs of the beam splitter, after passing though two 1-mm-size apertures (A) and long-pass filters (F) with cutoff wavelength 515 nm to remove the residual pump radiation, are focused into a multimode optical fiber and directed to two single-photon-counting detectors (EG&G, SPCM-AQR-15), D_1 and D_2. The typical distance between the 1 mm apertures and the output face of the crystal was about 70 cm. The coincidences of photons arriving at the two detectors are recorded within a time window determined by a coincidence circuit. The delay τ is swept and we monitor the coincidence rate $C(\tau)$ which is given by

$$C(\tau) = 1 - Re[\Lambda(2\tau)], \tag{8}$$

where

$$\Lambda(\tau) = \int d\Omega_s S(\Omega_s) e^{-i\Omega_s \tau}. \tag{9}$$

Thus, the spectral density can be easily obtained as the Fourier transform of the coincidence interferogram, and the spectral width will be inversely proportional to the width of the coincidence dip.

For the spectral characterization of the individual photons, the photons in beam 1 are discarded, and the photons in beam 2 are used as a low-coherence-time light source. The mirrors M_1 and M_2 are then used as a standard Michelson

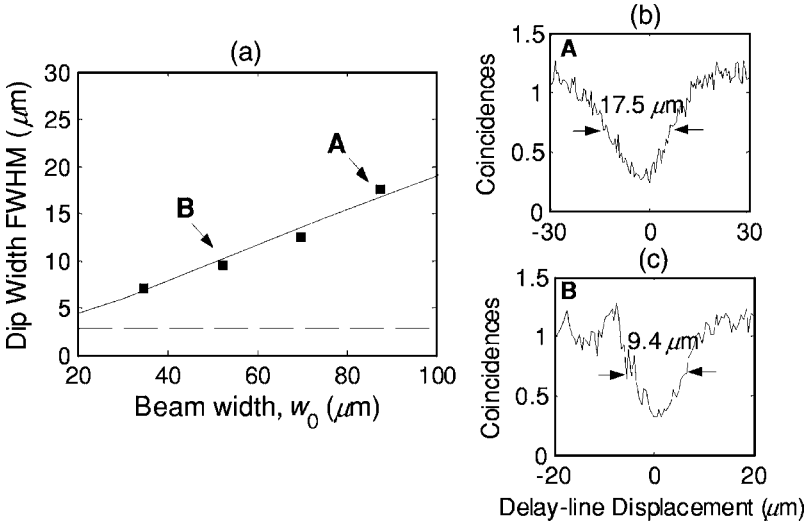

FIG. 3. (a) Measured width (FWHM) of the coincidence interferogram dip vs the pump beam width w_0 for a selected noncollinear angle $\varphi_1=-\varphi_2=5°$. The squares are the experimental results. The solid curve is the theoretical prediction obtained from Eq. (5). (b), (c) Details of the coincidence interferogram normalized to the constant background value for two different input beam waists, $w_0=87.4$ μm and $w_0=52.5$ μm, respectively, corresponding to points labeled as A and B in (a). The exposure time was 40 s per count, and the accidental counts were at a level of about 15%. The typical coincidence counting rates for these aperture sizes and exposure time were of the order of 10^3 counts.

interferometer. The reflections from both mirrors, recombined at beam splitter BS′, are collected at either of the two detectors. The temporal delay τ' introduced in mirror M_2 is swept and the single counts rate is recorded as the interferogram $I(\tau')$

$$I(\tau') = 1 - 2\,\mathrm{Re}[\Lambda(\tau')e^{-i\omega_s\tau'}]. \tag{10}$$

The spectrum of the individual photons can thus be obtained from the Fourier transform of the envelope of the interferogram.

The results for the joint-spectrum detection scheme are summarized in Fig. 3, where we have plotted the observed width [full width at half maximum (FWHM)] of the coincidence dip versus the input pump beam waist for a particular noncollinear internal angle $\varphi_1=-\varphi_2\simeq 5°$. The squares represent the experimental data, whereas the solid curve represents the theoretical calculation. The dashed line represents the theoretical upper limit obtained for the collinearly phase-matched configuration for this particular crystal. Two examples of the measured coincidence interferograms are shown at the right. It is clear from the figure that the dip width, and thus the spectral width, can be tailored via the properties of the pump beam. More sophisticated spectral shapes can be obtained by engineering the spatial shape of the input pump beam.

It is worth noting that for our specific experimental arrangement (detection apertures size, distance between the nonlinear crystal and the detectors, wavelengths, and noncollinear angle), the measured bandwidth corresponds to the value given by Eq. (5), only for focused pump beams ($\omega_0 \ll 600\ \mu$m), as shown in Fig. 3. For larger values of the pump beam waist, we have determined that the dip width reaches a saturation value that depends on the size of the detection aperture. In this case, the probability of detecting a signal photon with angular frequency $\omega_s^0+\Omega_s$, in coincidence

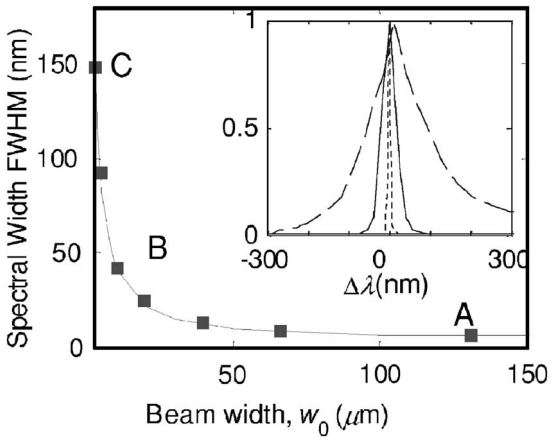

FIG. 4. Spectral width (obtained from the Fourier transform of the envelope of the interferogram) vs the pump beam width w_0, for a selected noncollinear angle $\varphi_1=-\varphi_2=9°$ in the single-photon detection scheme. The squares are the experimental results. The solid curve is the theoretical prediction obtained from Eq. (7). Inset: Detail of the measured spectral shape for three different input beam waists corresponding to points A, B, and C. The exposure time was 2 s per count, and the noise was at a level of 3%. The typical single counting rates for these aperture sizes and exposure time were of the order of 10^4 counts.

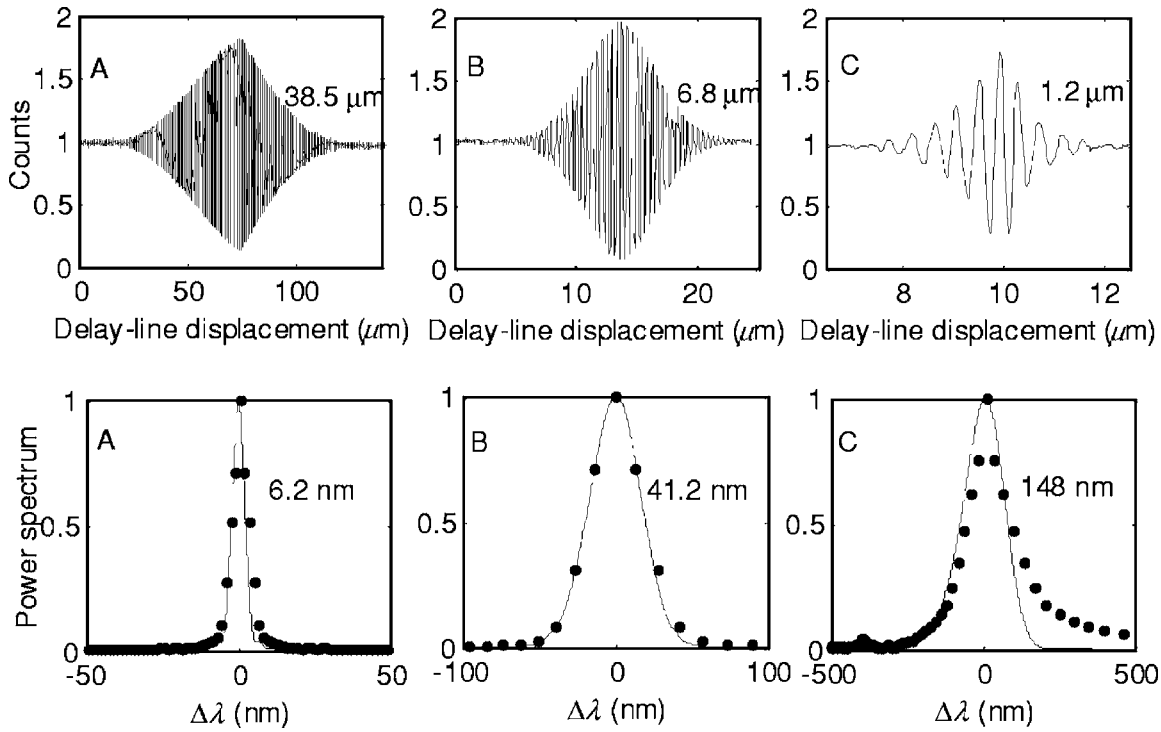

FIG. 5. (a) Measured interference fringes normalized to the constant background value, vs the displacement of the delay line, and (b) measured (circles) and theoretical (solid curve) power spectra for the three points labeled as A, B, and C in Fig. 4, corresponding to pump beam waists $w_0=131\ \mu$m, $w_0=10.5\ \mu$m, and $w_0=2.6\ \mu$m, respectively.

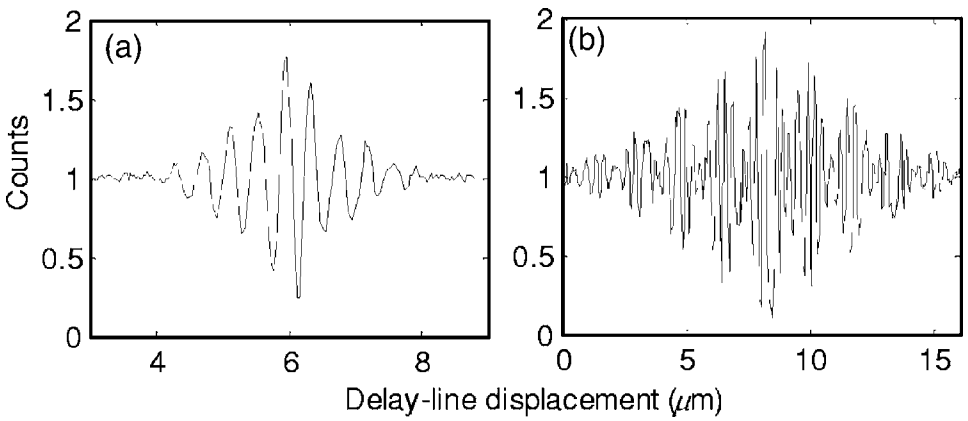

FIG. 6. Normalized interferograms for a noncollinear angle of $\varphi_1=-\varphi_2=5°$ and two different values of the pump beam waist: (a) $w_0=2.6\ \mu$m, and (b) $w_0=70\ \mu$m. The exposure time was 1 s per count.

with an idler photon with angular frequency $\omega_i^0-\Omega_s$, is strongly correlated with the transverse positions $\mathbf{x}_1$ and $\mathbf{x}_2$. Therefore, a correct theoretical description of the measured spectral bandwidth would require the consideration of the aperture size. Notwithstanding, one would recover the values given by Eq. (5) by using pinholes of smaller size.

The tailoring of the spectrum of the individual signal or idler photons, in the single-photon-count detection scheme, is displayed in Figs. 4 and 5. In Fig. 4, we have plotted the width of the spectrum (obtained by Fourier transforming the envelope of the interference pattern) versus the input pump beam waist, for a noncollinear angle of $\varphi_1=-\varphi_2\simeq 9°$. The solid curve represents the numerical calculation while the squares represent the experimental values. As expected from Fig. 1, a much larger spectral range is available in this case. The spectral width was tuned from 150 to 10 nm by simply changing the pump focusing lens.

The details of the measured interference fringes and the theoretical (solid curve) and experimental (circles) spectra are shown in Fig. 5 for three different pump beam waists, denoted A, B, and C in Fig. 4. Good agreement between experiment and theory is obtained. For larger spectral widths, the measured spectral shape begins to deviate from the one calculated theoretically, presumably because of the limited spectral response of the components of our setup, principally the detectors.

As we suggested earlier, multiple-peaked spectra of the individual signal and idler photons can be obtained, even when a simple Gaussian beam is used as the pump. This new degree of freedom is introduced by the integral in Eq. (7) over the momentum space of the discarded photon. For particular noncollinear angles, different pump beam waists allow us to tune the spectral shape from single peaked to multiple peaked. For example, for our particular configuration, this occurs for angles close to $\varphi_1=-\varphi_2\simeq 5°$. For this angle, in coincidences we expected a Gaussian-like joint spectrum, as predicted by Eq. (5) and demonstrated in Fig. 3. However, for the single-detection scheme, Eq. (7) predicts a broad single-peaked spectrum only for tightly focused beams, but a double-peaked spectrum when a broader pump is used. Typical measured interferograms, corresponding to a single-peaked and a multiple-peaked structure, for two different pump beam waists, are illustrated in Fig. 6.

IV. CONCLUSION

In conclusion, we have demonstrated that the use of noncollinearly phase-matched SPDC in suitable materials provides a powerful tool for managing the spectral width of two-photon quantum states. In particular, we have experimentally demonstrated the possibility of manipulating the spectrum of photon pairs by combining the use of noncollinear SPDC with proper spatial engineering of the input pump beam.

The results presented here are valid in the commonly used nearly collinear configurations, where the width of the pump beam can also noticeably change the spectral width of the down converted photons, a feature that should be taken into account when devising practical schemes for enhancing the amount of entanglement in polarization and spatial-entanglement protocols. Both the joint spectrum of the entangled-photon pairs and the individual spectrum of the signal or idler photons can be tailored by using this method.

ACKNOWLEDGMENTS

This work was supported by the Fulbright Program and the Spanish Ministry of Education and Science; by the Grant No. FIS2004-03556 from the Government of Spain; by the Generalitat de Catalunya; by the European Commission under the Integrated Project Qubit Applications (QAP) funded by the IST directorate as Contract No. 015848; by the Center for Subsurface Sensing and Imaging (CenSSIS), a U.S. National Science Foundation Engineering Research Center; by a U.S. Army Research Office (ARO) Multidisciplinary University Research Initiative (MURI) Grant; and by the David and Lucile Packard Foundation. The authors are grateful to M. B. Nasr for valuable discussions.

[1] *The Physics of Quantum Information*, edited by D. Bouwmeester, A. Ekert, and A. Zeilinger (Springer-Verlag, Berlin, 2000).
[2] B. E. A. Saleh, A. F. Abouraddy, A. V. Sergienko, and M. C. Teich, Phys. Rev. A **62**, 043816 (2000).
[3] K. Mattle, H. Weinfurter, P. G. Kwiat, and A. Zeilinger, Phys. Rev. Lett. **76**, 4656 (1996).
[4] D. Bouwmeester and J.-W. Pan, Nature (London) **390**, 575 (1997).
[5] K. Mattle, H. Weinfurter, P. G. Kwiat, and A. Zeilinger, Phys. Rev. Lett. **76**, 4656 (1996).
[6] T. B. Pittman, D. V. Strekalov, D. N. Klyshko, M. H. Rubin, A. V. Sergienko, and Y. H. Shih, Phys. Rev. A **53**, 2804 (1996).
[7] A. Joobeur, B. E. A. Saleh, and M. C. Teich, Phys. Rev. A **50**, 3349 (1994).
[8] A. F. Abouraddy, B. E. A. Saleh, A. V. Sergienko, and M. C. Teich, J. Opt. Soc. Am. B **19**, 1174 (2002).
[9] C. H. Monken, P. H. Souto Ribeiro, and S. Pádua, Phys. Rev. A **57**, 3123 (1998).
[10] A. Vaziri, J. W. Pan, T. Jennewein, G. Weihs, and A. Zeilinger, Phys. Rev. Lett. **91**, 227902 (2003).
[11] S. P. Walborn, A. N. de Oliveira, S. Pádua, and C. H. Monken, Phys. Rev. Lett. **90**, 143601 (2003); B. E. A. Saleh, A. Joobeur, and M. C. Teich, Phys. Rev. A **57**, 3991 (1998); A. F. Abouraddy, B. E. A. Saleh, A. V. Sergienko, and M. C. Teich, J. Opt. B: Quantum Semiclassical Opt. **3**, S50 (2001).
[12] W. P. Grice, R. Erdmann, I. A. Walmsley, and D. Branning, Phys. Rev. A **57**, R2289 (1998).
[13] Z. Y. Ou and Y. J. Lu, Phys. Rev. Lett. **83**, 2556 (1999).
[14] M. Bellini, F. Marin, S. Viciani, A. Zavatta, and F. T. Arecchi, Phys. Rev. Lett. **90**, 043602 (2003).
[15] S. Viciani, A. Zavatta, and M. Bellini, Phys. Rev. A **69**, 053801 (2004).
[16] A. Pe'er, B. Dayan, A. A. Friesem, and Y. Silberberg, Phys. Rev. Lett. **94**, 073601 (2005).
[17] N. Gisin, Rev. Mod. Phys. **74**, 145 (2002).
[18] A. F. Abouraddy, M. B. Nasr, B. E. A. Saleh, A. V. Sergienko, and M. C. Teich, Phys. Rev. A **65**, 053817 (2002); M. B. Nasr, B. E. A. Saleh, A. V. Sergienko, and M. C. Teich, Phys. Rev. Lett. **91**, 083601 (2003); M. B. Nasr, B. E. A. Saleh, A. V. Sergienko, and M. C. Teich, Opt. Express **12**, 1353 (2004).
[19] D. Branning, W. P. Grice, R. Erdmann, and I. A. Walmsley, Phys. Rev. Lett. **83**, 955 (1999).
[20] V. Giovannetti, S. Lloyd, and L. Maccone, Nature (London) **412**, 417 (2001); V. Giovannetti, L. Maccone, J. H. Shapiro, and F. N. C. Wong, Phys. Rev. Lett. **88**, 183602 (2002).
[21] W. P. Grice, A. B. URen, and I. A. Walmsley, Phys. Rev. A **64**, 063815 (2001).
[22] S. Carrasco, J. P. Torres, L. Torner, A. Sergienko, B. E. A. Saleh, and M. C. Teich, Phys. Rev. A **70**, 043817 (2004).
[23] A. De Rossi and V. Berger, Phys. Rev. Lett. **88**, 043901 (2002).
[24] M. C. Booth, M. Atatüre, G. Di Giuseppe, B. E. A. Saleh, A. Sergienko, and M. C. Teich, Phys. Rev. A **66**, 023815 (2002).
[25] Z. D. Walton, M. C. Booth, A. V. Sergienko, B. E. A. Saleh, and M. C. Teich, Phys. Rev. A **67**, 053810 (2003).
[26] A. B. URen, K. Banaszek, and I. A. Walmsley, Quantum Inf. Comput. **3**, 480 (2003).
[27] J. P. Torres, C. I. Osorio, and L. Torner, Opt. Lett. **29**, 1939 (2004).
[28] B. E. A. Saleh and M. C. Teich, *Fundamentals of Photonics* (Wiley, New York, 1991), Chap. 4.
[29] S. Carrasco, M. B. Nasr, A. V. Sergienko, B. E. A. Saleh, J. P. Torres, and L. Torner, Opt. Lett. **31**, 253 (2006).